Remote Sens. **2015**, *7*, 4948-4967; doi:10.3390/rs70404948

OPEN ACCESS

remote sensing

ISSN 2072-4292

www.mdpi.com/journal/remotesensing

Article

Knowledge-Based Detection and Assessment of Damaged Roads Using Post-Disaster High-Resolution Remote Sensing Image

Jianhua Wang [1], Qiming Qin [1,*], Jianghua Zhao [2], Xin Ye [1], Xiao Feng [1], Xuebin Qin [1] and Xiucheng Yang [1]

[1] Institute of Remote Sensing and Geographic Information System, Peking University, Beijing 100871, China; E-Mails: wjhdg@163.com (J.W.); lanlang524@126.com (X.Y.); fengxiao198995@163.com (X.F.); qxbsdnd@163.com (X.Q.); xiuchengyang@163.com (X.Y.)

[2] Scientific Data Center, Computer Network Information Center, Chinese Academy of Sciences, Beijing 100190, China; E-Mails: zjh@cnic.cn

* Author to whom correspondence should be addressed; E-Mail: qmqin@pku.edu.cn; Tel.: +86-10-6276-4430.

Academic Editors: Gonzalo Pajares Martinsanz and Prasad S. Thenkabail

Received: 23 January 2015 / Accepted: 20 April 2015 / Published: 22 April 2015

Abstract: Road damage detection and assessment from high-resolution remote sensing image is critical for natural disaster investigation and disaster relief. In a disaster context, the pairing of pre-disaster and post-disaster road data for change detection and assessment is difficult to achieve due to the mismatch of different data sources, especially for rural areas where the pre-disaster data (*i.e.*, remote sensing imagery or vector map) are hard to obtain. In this study, a knowledge-based method for road damage detection and assessment solely from post-disaster high-resolution remote sensing image is proposed. The road centerline is firstly extracted based on the preset road seed points. Then, features such as road brightness, standard deviation, rectangularity, and aspect ratio are selected to form a knowledge model. Finally, under the guidance of the road centerline, the post-disaster roads are extracted and the damaged roads are detected by applying the knowledge model. In order to quantitatively assess the damage degree, damage assessment indicators with their corresponding standard of damage grade are also proposed. The newly developed method is evaluated using a WorldView-1 image over Wenchuan, China acquired three days after the earthquake on 15 May 2008. The results show that the producer's accuracy (PA) and user's accuracy (UA) reached about 90% and 85%, respectively, indicating that

the proposed method is effective for road damage detection and assessment. This approach also significantly reduces the need for pre-disaster remote sensing data.

Keywords: high-resolution remote sensing image; road centerline; knowledge model; damage detection; assessment indicator

1. Introduction

There are various types of disasters, and the disasters are widely distributed across the world with high frequency, which result in heavy loss in economy and social stability [1]. As a key component of the transportation systems, roads play a significant role in lifeline engineering in the disaster prevention and mitigation [2–4]. Road damage is mainly caused by the surrounding terrain, geology, hydrology and other environmental changes. Road damage detection and assessment consist to identify the damaged roads and evaluate the traffic capacity of road after disaster. It facilities the early assessment of disasters, urgent repair of lifeline systems and the reconstruction of transportation infrastructures, and also improves the efficiency of disaster rescue [5–8].

Before the advent of remote sensing technology, disaster assessment relied on field investigation [9–11]. The United States divides the process of damage assessment into two parts: early assessment and on-site assessment. The early assessment depends on the assessment results of HAZUS-MH system and the aerial photos of satellite, helicopter or unmanned aerial vehicle, which provide technical support for disaster relief. The on-site assessment is accomplished by professionals or trained volunteers according to assessment handbooks and relevant technical documentations [12–16]. As an earthquake-prone country, Japan has accumulated rich experience in disaster assessment. The road disaster assessment and emergency response techniques of Japan are similar to those of the United States. In Japan, the entire process of road disaster emergency and reconstruction consists of three phases: urgent investigation and urgent measurements phase, emergency restoration phase and reconstruction phase [17,18]. China initiated the study on disaster prevention and mitigation later than those developed countries. The road disaster assessment is generally based on previous experience and fuzzy theory [19]. With the development of remote sensing technology, we can get more information about the spatial ground features, detailed textures and other information from remote sensing images [20,21]. Remote sensing has been widely applied on road extraction and damage detection.

In terms of road extraction, Kaur *et al.* [22] gave an informative review of various road extraction methods, fundamentally branching into three stages: image pre-processing, road detection and post-processing. Some applications of semi-automatic road extraction methods were reviewed by Li *et al.* [23]. According to different processing methods, recent road extraction techniques can be mainly classified into a few groups, such as line-based [24], region-based [25], and knowledge-based techniques [26]. Trinder *et al.* proposed a knowledge-based method for automatic road extraction from aerial images, in which the geometric and radiometric properties of roads and the relationship between roads in low and high resolution images are formulated as rules and stored in the knowledge base. The road network can be successfully extracted by the proposed method [27]. Based on normalized cut algorithm and texture progressive analysis, Senthilnath *et al.* put forward a road extraction method

with respect to geometric, structural and spectral characteristics of roads. The method is efficient in extracting road segments in urban region from high resolution satellite images [28]. The adaptive global threshold and the morphological operations are used to extract road network from high resolution satellite image by Pankaj. The method can be used in reliable way for automatic extraction of roads from high-resolution satellite image. However, there is a chance that a small part of barren land or parking area could be mistakenly classified as roads in some cases [29]. With the circular projection transformation, a novel road extraction algorithm using high resolution remote sensing images is proposed and it can extract different levels of roads from high-resolution remote sensing images effectively [30]. All the aforementioned methods can be applied in road extraction. However, most of the techniques are not applied on both urban and rural area road images. Also, the color of roof tops that is analogous to that of roads may result in improper extraction of roads.

For road damage detection, Gong *et al.* presented a road damage extraction approach based on the method of object-oriented change detection with road vector data overlaid on post-earthquake image, and the capacity of road damage monitoring from high resolution remote sensing images is confirmed [31]. Ma *et al.* developed a road damage detection system that uses the basic road data in GIS (Geographical information system) as the prior knowledge to detect damaged roads [32,33]. Samadzadegan used the pre-disaster and post-disaster data to detect damaged roads and gained promising results by fuzzy inference systems [34,35]. Haghighattalab *et al.* adopted a similar method that used the vector map and post-disaster satellite images for road damage detection in Bam, Iran [36]. In summary, most of the existing studies focus on road damage detection using both the pre-disaster data and post-disaster image. However, few studies have been conducted on road damage detection and assessment using remote sensing and even less for research without the pre-disaster data.

To overcome the aforementioned problems, this paper proposes a knowledge-based method for road damage detection and assessment using high-resolution remote sensing images, which compensates the absence of pre-disaster data. The aims of this study are: (1) extracting the post-disaster roads for the normal operation and regulation of transportation systems, (2) detecting damaged roads for disaster rescue, (3) assessing damaged roads for road rebuilt, and (4) setting standard for road damage grade for future reference.

2. Methods

This study proposes a method of road damage detection and assessment based on road knowledge. There are four key procedures in this study: the road centerline extraction, the post-disaster road extraction, the damage detection and the damage assessment. Road centerline is identified from high-resolution remote sensing images firstly and is used to extract the post-disaster roads with the knowledge model. Damaged roads are detected by the spatial analysis, and road damage assessment is conducted on the basis of the assessment model. Figure 1 illustrates the detailed procedures.

2.1. Road Centerline Extraction

A disaster can turn the boundary of the road into an irregular polygon. The existing methods of road extraction are relatively hard to be applied in practical damage detection and assessment [37,38]. In this case, road centerline plays a critical role in road damage detection and assessment. Miao *et al.* put

forward an integrated method incorporating the strengths of the geodesic method, kernel density estimation (KDE), and mean shift to extract the road centerline [39]. This method is based on the preset road seed points with no need for complete road information and is adopted in this paper. This method consists of three main steps. Firstly, a geodesic method [40] is used to extract the initial road segments that link the seed points. Secondly, a road probability is calculated based on these coarse road segments. A threshold operation is then applied to separate the remote sensing image into two categories: the road and non-road classes [41]. Next, a kernel density estimation map is generated using the road class image with the KDE. Let $y_1, y_2, ..., y_n$ be given set of d-dimensional random samples. The KDE is defined as [39,42]:

$$f(y) = \frac{1}{nh^d} \sum_{i=1}^{n} K\left(\frac{y - y_i}{h}\right) \quad \left(K(y) = e^{-\frac{y^2}{2h^2}}\right) \tag{1}$$

where n is the number of observations, h denotes the bandwidth parameter (which is determined by generalizing Scott's rule of thumb [42]), and K is the kernel function. Then, the mean shift method is used to obtain precise centered positions of the road. The mean shift is defined as [43]

$$\mathrm{m}(y) = \frac{\Sigma_{i=1}^{n} \mathrm{g}\left(\frac{y - y_i}{h}\right) y_i}{\Sigma_{i=1}^{n} \mathrm{g}\left(\frac{y - y_i}{h}\right)} - y \quad \left(g(y) = -K'(y)\right) \tag{2}$$

where $K'(y) = -\frac{y}{h^2} \cdot e^{-\frac{y^2}{2h^2}}$. After obtaining the precise road seed points, the geodesic method is used once again to link the seed points. The line that links the seed points is determined as the road centerline.

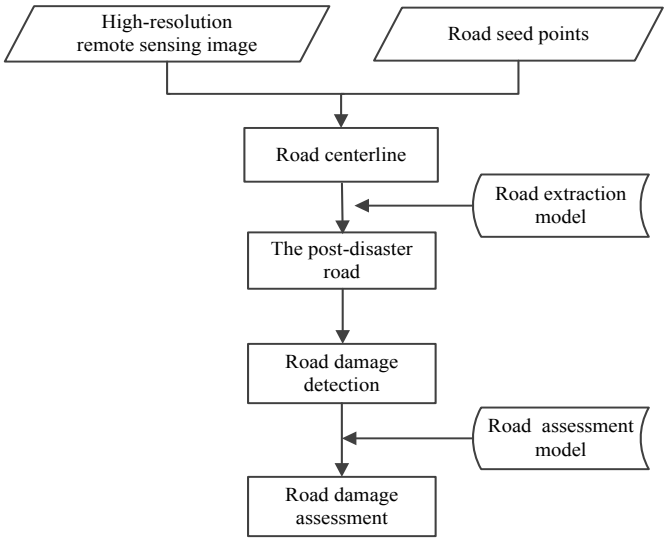

Figure 1. Flow chart of road damage detection and assessment.

2.2. Post-Disaster Road Extraction Based on Knowledge

The representation and extraction of road knowledge is critical to extracting the post-disaster roads. In general, the roads in the high-resolution remote sensing images usually present features specified as follows (Figure 2a): (1) Roads are ribbon-shaped with steady width. (2) The road objects generated by

road segmentation (multi-scale segmentation) show relatively high homogeneity. (3) The two edges (sidelines) of roads are usually parallel and distinctive in images. (4) Roads have regular geometry, and their rectangularity and the length-to-width ratio are high. With occurrence of the disaster, the roads can be divided into undamaged and damaged road segments. As compared with the pre-disaster roads, the undamaged road segments remain the same, while the boundary of damaged road segments turns into an irregular polygon (Figure 2b).

The post-disaster road refers to the undamaged road and it means the part of road that has not been damaged after the disaster. Because the damaged road is irregular, it is very difficult to be extracted directly. In this study, the post-disaster road is used to detect the damaged road. A knowledge-based method is proposed for post-disaster road extraction. This method consists of four main steps. Firstly, the width of a road is calculated using the road centerline and the road edges obtained by the edge detection method. Then, appropriate road knowledge is chosen to build the knowledge model for road extraction. It includes the hypothesis model and the verification model. Successively, hypothesized road segments are extracted using the hypothesis model under the guidance of the road centerline, and finally the verification model is used to verify the hypothesized road segments. The results after verification are post-processed by mathematical morphology, and the post-disaster road segments are extracted.

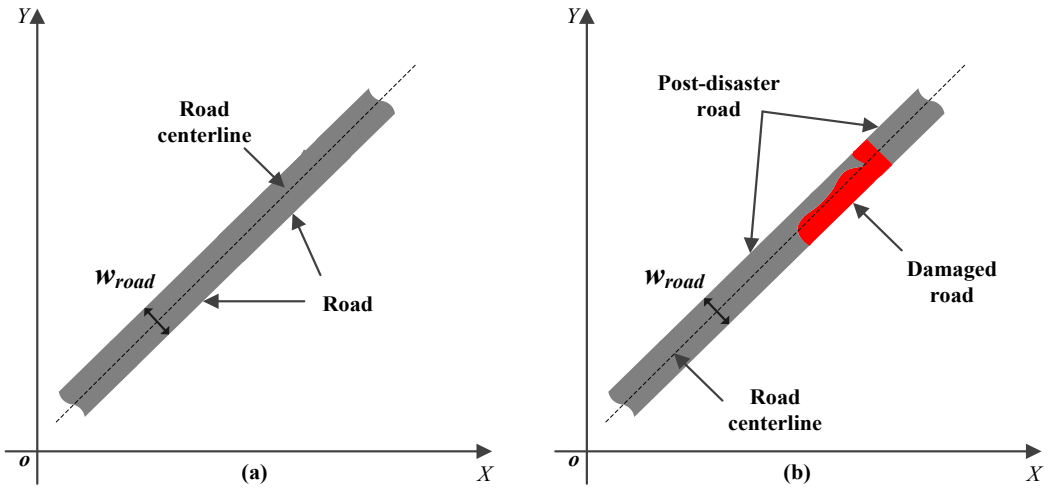

Figure 2. The diagram of road. (**a**) The road before disaster; (**b**) The road after disaster.

In this study, the road centerline and road edges are selected to calculate the road width w_{road}. The bilateral filter is used to highlight the road edges so as to preserve the edges. It is defined as [44]

$$BF[\mathrm{I}]_p = \frac{1}{W_p}\sum_{q\in s} G_{\sigma_s}(\|\mathrm{p}-\mathrm{q}\|)G_{\sigma_r}(|\mathrm{I}_p-\mathrm{I}_q|)\mathrm{I}_q \tag{3}$$

where normalization factor W_p ensures the sum of pixel weights equals to 1.0. I is the image. The p is the center position, and the weight G_{σ_s} for pixel q is defined by the Gaussian $G_{\sigma_s}(\|\mathrm{p}-\mathrm{q}\|)$ [44]. G_{σ_r} is a range Gaussian that decreases the influence of pixel q when the intensity value $\mathbf{I}_q$ differs from $\mathbf{I}_p$ [44]. In order to detect the road edges, the canny edge detection algorithm [45] is applied after edges are highlighted by bilateral filter. The gradient direction [45] in the procedure of canny edge detection is defined as:

$$n = \frac{\nabla(\mathrm{G}^{*}\mathrm{I})}{|\nabla(\mathrm{G}^{*}\mathrm{I})|} \tag{4}$$

where n is the gradient direction, * denotes convolution, I is the image and G is the two-dimensional Gaussian [45]. Because the width of a road remains invariant, we can still calculate the road width when the detected edges are incomplete. The road width is then obtained by combining the road centerline with detected edges.

Quantitative parameters of road knowledge include brightness, standard deviation, rectangularity, area, length-to-width ratio and so on. The knowledge-based method has two key components: hypothesis generation and verification of hypotheses. The hypothesis model is built for hypothesis generation and the verification model is built to verify the hypotheses. The brightness and standard deviation are selected to build the hypothesis model and the rectangularity and length-to-width ratio are selected to build the verification model. The expression of the hypothesis model is as follows:

$$H_{road} = B_{road} \bigcup_{road} \left(b_1 \le B_{road} \le b_2 \ \ or \ \ s_1 \le S_{road} \le s_2\right) \tag{5}$$

where H_{road} is the hypothetic road segments, B_{road} and S_{road} are the brightness and standard deviation of the road segments, respectively, b_1 and b_2 are the predefined thresholds for the brightness of the road segments, s_1 and s_2 are the predefined thresholds for the standard deviation of the road segments. For the objects generated by image segmentation, if $B_{road} \in [b_1, b_2]$ or $S_{road} \in [s_1, s_2]$, the corresponding objects are defined as hypothetic road segments. Nevertheless, there are still some trees, vehicles and other false objects in the hypothetic road segments. The verification model is used to remove those false objects. The expression of verification model is as follows:

$$V_{road} = H_{road} - R \bigcup \left(R < r_1 \ \ or \ \ W < w_1\right) \tag{6}$$

where V_{road} is the road segments after verification, R and W are the rectangularity and length-to-width ratio of the road segments, respectively, r_1 and w_1 are the predefined thresholds for the rectangularity and length-to-width ratio of the road segments, respectively. Equation (6) means that for the objects in hypothetic road segments, if $R \in (0, r_1)$ or $W \in (0, w_1)$, the corresponding objects are removed from the H_{road}. The verified results are the road segments.

For the post-disaster road segments, the knowledge model built foregoing is used to extract them after the multi-scale segmentation by the object-oriented method. The specific principle is shown in Figure 3.

Figure 3 shows the schematic diagram of post-disaster road extraction. The procedure for extracting the post-disaster road segments is as follows:

(1) l is bisected vertically by the road centerline. Starting from p_1, the road objects intersected by l at p_1 are examined by the hypothesis model.

(2) If they pass the hypothesis model, they are classified as hypothetic road segments and *vice versa*.

(3) If the hypothetic road segments are identified, they are to be verified by the verification model and the false road objects will be removed, otherwise the next pixel p_2 is analyzed.

(4) After traversing all the pixels in P, the extracted results will be post-processed by the closing operation of mathematical morphology, which is used to reduce the influence of trees, vehicles and other landmarks. The structuring element was chosen to be a disc with radius r of 2. With the

structuring element at this scale, roads will not be adversely affected. In this way, the post-disaster road segments are extracted.

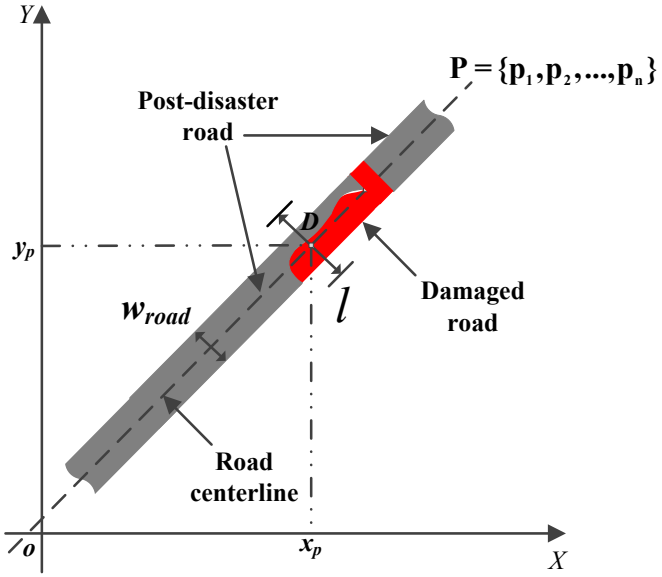

Figure 3. Schematic diagram of post-disaster road extraction. P is a group of pixels located in the road centerline ($P=\{p_1,p_2,...,p_n\}$, n is the total number of pixels). l represents the searching line which moves along the road centerline and the length is D ($D \geq w_{road}$).

The proposed models are tested and subsequently validated using an urban image without damage. It can be seen from Figure 4 that (a) is the test image with the resolution of 0.1 m, (b) shows the hypothetic roads generated by the hypothesis model and the roads verified by the verification model are shown in (c). The producer's accuracy (PA) and user's accuracy (UA) are 95.14% and 90.34%, respectively, indicating that the proposed models can effectively extract the road without damage.

(**a**) (**b**) (**c**)

Figure 4. Road extraction. (**a**) The test image, which is an urban image without damage; (**b**) The hypothetic roads; (**c**) The roads after verification.

2.3. Road Damage Detection Using the Spatial Analysis

In this paper, damaged road is detected using the spatial relationship between the post-disaster road and damaged road. With occurrence of the disaster, the roads are divided into post-disaster roads and

damaged roads. The spatial relationship between the post-disaster road and damaged road is adjacent but do not intersect (Figure 2b). The buffer with the radius of $w_{road}/2$ is generated by the road centerline. By applying the ERASE operation to the buffer with the post-disaster roads, the damaged road is obtained. The ERASE operation is one of the spatial overlay analysis methods. The function of the ERASE operation is as follows:

$$D = A - B \tag{7}$$

where D is the damaged road, A and B are the pre-disaster and post-disaster road. The function means that $D \in A \ \ and \ \ D \notin B$. The schematic diagram of road damage detection is shown in Figure 5. A, B and D refer to pre-disaster road, post-disaster road and damaged road, respectively.

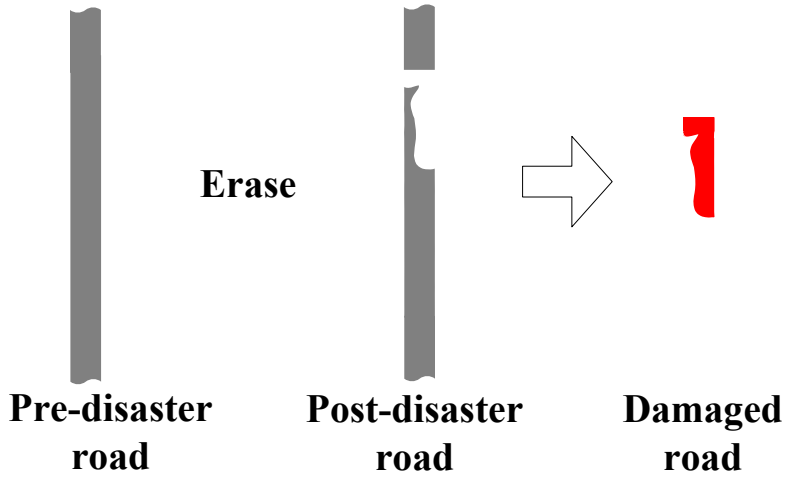

Figure 5. Schematic diagram of road damage detection.

2.4. Building Indicators of Road Damage Assessment

Road damage assessment using the high resolution optical remote sensing images is only based on the variation of pavement when there is no other auxiliary data. In this study, the indicators of road damage assessment are built based on the road width, length, area and relative parameters of damaged road obtained from damage detection. The indicators are shown as follows:

(1) Damaged width and damaged ratio of width

Damaged width refers to the width of a damaged road, and it is denoted by $w_{damaged}$. It reflects the damaged extent of traffic capacity of the road.

Damaged ratio of width refers to the ratio between the width of a damaged road and the width of the full road. It reflects the damaged extent of the road in width. The computation is as follows:

$$\rho_w = \frac{w_{damaged}}{w_{full}} \tag{8}$$

where, ρ_w refers to damaged ratio of width, and w_{full} refers to the width of the full road.

(2) Damaged length and damaged ratio of length

Damaged length refers to the length of a damaged road and it is denoted by $L_{damaged}$. It reflects damaged scale of the road.

Damaged ratio of length refers to the ratio between the length of a damaged road and the length of the full road. It reflects the damaged extent of the road in length. The computation is as follows:

$$\rho_L = \frac{L_{damaged}}{L_{full}} \tag{9}$$

where, ρ_L refers to damaged ratio of length, and L_{full} refers to the length of the full road.

(3) Damaged area and damaged ratio of area

Damaged area refers to the area of a damaged road and it is denoted by $A_{damaged}$. It reflects damaged size of the road.

Damaged ratio of area refers to the ratio between the area of a damaged road and the area of the full road. It reflects the damaged extent of the road in area. The computation is as follows:

$$\rho_A = \frac{A_{damaged}}{A_{full}} \tag{10}$$

where, ρ_A refers to damaged ratio of area, and A_{full} refers to the area of the full road.

2.5. Setting Standard for Road Damage Grade Classification

The damage grade is the classification of damage degree and is critical to damage assessment and disaster management. In addition, it is also one of the hot issues of disaster theory [46]. At present, the methods of damage grade classification include arc discrimination, logarithmic function, ratio, weighted accumulation, matter-element analysis, gray relational analysis, gray clustering and fuzzy discrimination [47–49].

Road damage grade is an important component of the disaster grade and is significant to assessing the damage degree of the transport systems and lifeline engineering. In the United States, road damage grade is divided into five grades: *none, slight, moderate, extensive* and *irreparable* [50]. In China, five grades are also identified based on the structure damage ratio of lifeline systems engineering, including *basic, minor, moderate, major* and *destructive* [51].

The damaged width, length and area all reflect the damage degree of a road. Moreover, the damaged ratio of width is the most important indicator to determine the capacity of a road, while the damaged ratio of length and areas reflects the damaged extent of a road. Considering the actual road capacity, and the existing standards of damage grade domestic and overseas, this study proposes a set of standard for road damage grade classification based on the damaged ratio of width (ρ_w). Table 1 summarizes the standard of road damage grade.

Table 1. The standard of road damage grade.

Damage Grade	Damaged Ratio of Width: ρ_w (%)	Description
Basic	$0 \le \rho_W \le 10$	No significant changes in the pavement, and the safe passage of pedestrians and vehicles is unaffected.
Minor	$10 < \rho_W \le 30$	Pavement is partially buried by landslides or mudslides. A little operation is needed to restore to normal.
Moderate	$30 < \rho_W \le 50$	Localized moderate cracking. Reduced structural integrity of pavement. Repair is needed to continue to use it.
Major	$50 < \rho_W \le 100$	Failure of pavement structure. It cannot guarantee the safe passage of pedestrians and vehicles. It needs to be rebuilt.

3. Study Area and Data

3.1. Study Area

The study area (Figure 6) is located in the Wenchuan County, Sichuan Province, China. The Wenchuan County is located in the northwest edge of the Sichuan Basin, with Qionglai Mountain and the Longmen Mountain lying in the southwest and northeast of the county, respectively. Minjiang River, Zagunao River, Caopo River and Shoujiang River are the main rivers in this region [52]. The county is 84 km wide from east to west and 105 km long from north to south. Its coordinates range are 30°45′N–31°43′N, 102°51′E–103°44′E.

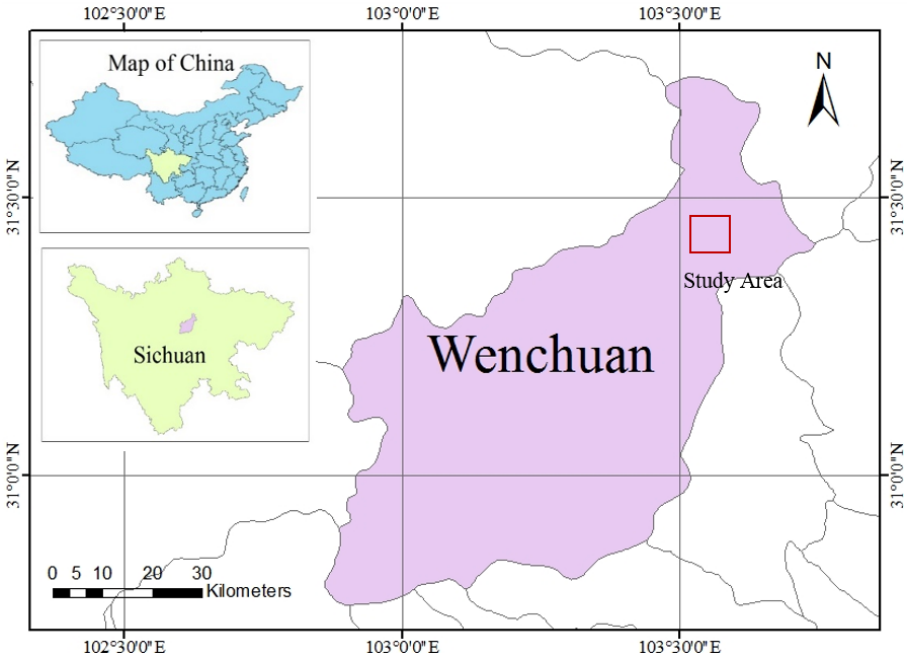

Figure 6. The spatial location of the study area.

A magnitude 8 earthquake occurred in Sichuan Province on 12 May 2008. It is called the "Wenchuan Earthquake". The epicenter is located in Wenchuan (31°0′N, 103°24′E) and the focal depth is 14 km. The meizoseismal area is a narrow strip along the causative fault to the Northeast extension. The earthquake is the most devastating one since the founding of New China with stricken area of more than 100,000 km^2. The magnitude, aftershocks, and secondary disasters are rare in the world and caused a huge loss to the lives and property of people. There were 69,227 deaths, 374,640 injured, and 17,923 people missing [52]. The number of victims who were in need of emergency resettlement and transfer is 15,100,000. A large number of houses collapsed. Roads, bridges and other infrastructures were damaged over large areas. Industrial and agricultural production suffered heavy losses, and the ecological environment also had been severely damaged.

3.2. Data Source

In this paper, the experimental data is a panchromatic remote sensing image (Figure 7) which was acquired by WorldView-1 on 15 May 2008. It was provided by the national disaster reduction center of

China. The spatial resolution is 0.5 m. The area covers 4290 pixels × 2851 pixels and its center coordinates are 103°32′52″E, 31°26′56″N.

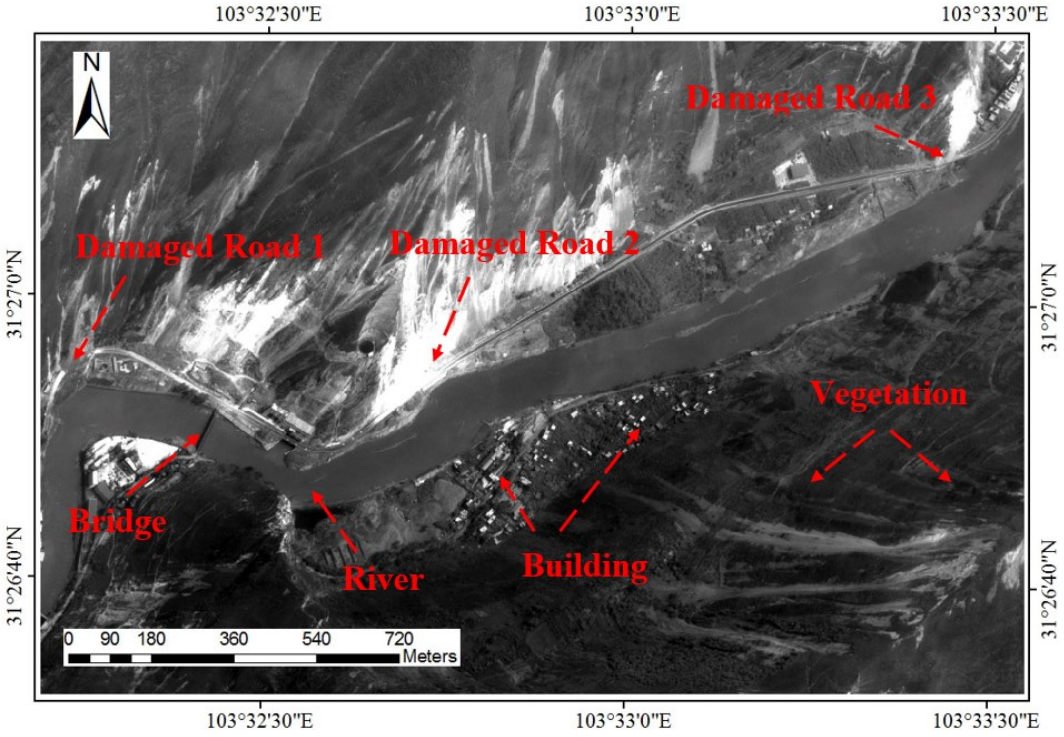

Figure 7. Image of WorldView-1 in the study area.

There are mountains, rivers, roads, bridges, buildings and other surface features in Figure 7. Road is an important part of transport systems along the river. Mountains are covered by vegetation with obvious shadows. Influenced by the strong shock waves, the deformation and earthquake induced landslides and mudslides, three road sections have been damaged. The road section 2 is severely blocked and buried by falling sediments and it is considered as the damaged road according to its traffic capacity.

4. Results and Discussions

4.1. Road Damage Detection

In this paper, the detection of damaged road is based on post-disaster road recognition. The process mainly includes road centerline extraction combining with road seed points, post-disaster road extraction based on knowledge and damage detection using spatial analysis.

The initial road segments that link road seed points are extracted by the geodesic method [39,40]. The initial road segments are taken as training samples. The Mahalanobis distance is used to measure the probability of a pixel belonging to the road class [41]. Then, the KDE technology [42] is applied to calculate the probability of any given pixel lying on the road centerline, and the precisely centered positions of road is determined through the mean shift method [43]. Finally, the geodesic method is used once again to link the seed points to form the refined centerline (Figure 8).

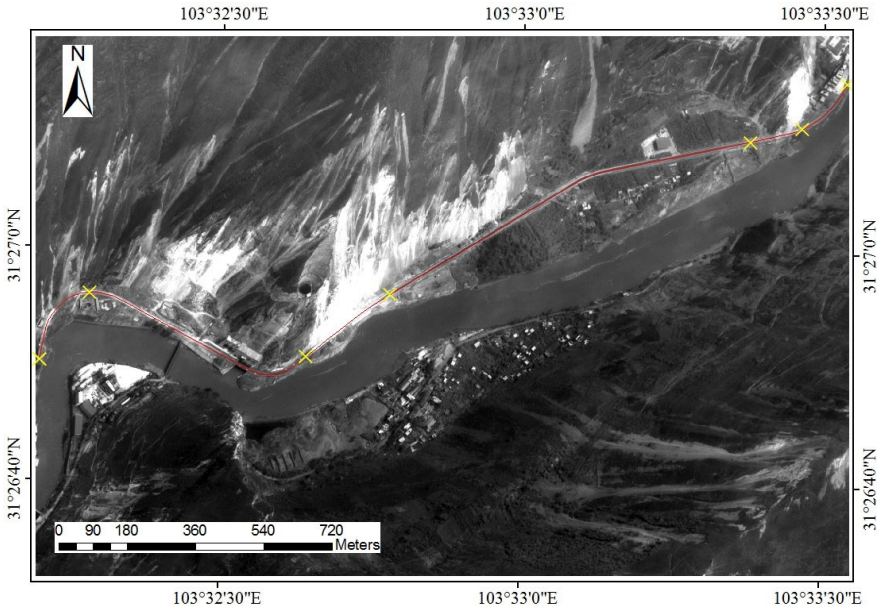

Figure 8. Result of road centerline extraction. The road centerline is shown as red line and the road seed points are shown as yellow crosses.

The road edges in the remote sensing image are highlighted by the bilateral filter [44]. The canny edge detection algorithm [45] and the road centerline are used to calculate the road width w_{road}, which is 15 pixels. The multi-scale segmentation method is used in image segmentation. The segmentation scale selection plays a critical role in image segmentation and in this study it is mainly related to the road width in the image. In general, the segmentation scale and road width w_{road} are positively correlated. In this paper, the segmentation scale was set to 10, 20, ... , 50 according to the analysis of image characteristics analysis. After some trial and error, the proposed extraction method with the segmentation scale of 30 that performs best on the integrity of the road objects. The optimal segmentation scale would be larger than 30 when the road width is thicker than 15 pixels and *vice versa.* Moreover, based on lots of experiments, we got an empirical conclusion that the optimal segmentation scale is usually in the scope of $(2 \pm 0.5)w_{road}$, which be used as a determination of the general range of optimal segmentation scale. After the image segmentation, the road objects are generated.

The post-disaster road segments are extracted based on the hypothesis model and the verification mode. Then, they are post-processed by closing operation of mathematical morphology. The results are shown in Figure 9. It can be seen from Figure 9 that the post-disaster road segments are identified accurately. In this process, the length of the searching line D is 20 pixels. D is set more than the road width w_{road} as the integrity of the road edges must be ensured. The width of extracted post-disaster road is slightly larger than the actual width, but it is significant in terms of improving the accuracy of damage detection.

After the post-disaster road extraction, the buffer with the radius of $w_{road}/2$ is generated by the road centerline and the erase analysis is used to detect the damaged regions of the road. The detection results of damaged roads are shown in Figure 10. It can be seen from Figure 10 that all the damage has been detected. However, some trees, vehicles, sands and gravels are detected as the damaged regions due to the spectral similarity of different objects, which has a small yet insignificant influence on the overall accuracy.

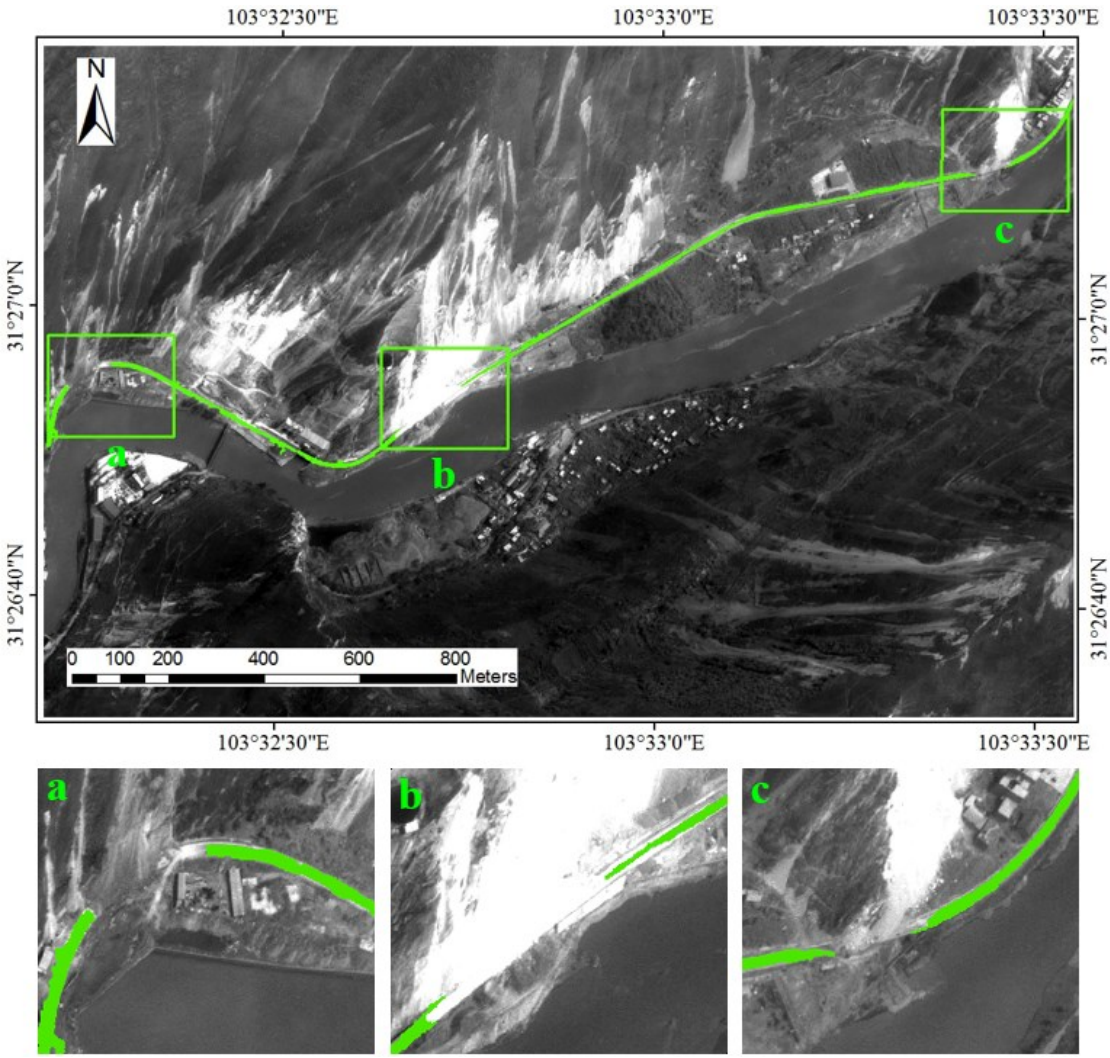

Figure 9. Results of post-disaster road extraction. Green regions are the post-disaster roads.

4.2. Accuracy Evaluation

Within the study area, the damaged road segments were also manually delineated. The width, length and area of the manually delineated results were calculated and used as references to assess the accuracy of the automatic damaged detection. Table 2 presents the accuracy of road damage detection.

Table 2. Accuracy evaluation of road damage detection.

Indicators	Real Damaged Road	Detected Damaged Road	Correctly Detected Road	PA (%)	UA (%)
Width	8m	7.5m	7.5m	93.75	100.00
Length	353m	392m	323m	91.50	82.40
Area	2661 m^2	2809 m^2	2322 m^2	87.26	82.66

PA: producer's accuracy; UA: user's accuracy.

It can be seen from Table 2 that the detection results are fairly accurate, which justifies the effectiveness of this method. The PA and UA can reach, on average, 90% and 85%, respectively. The newly proposed method does not require the pre-disaster data and achieves comparable results with existing methods, in which high accuracies were acquired from the pre-disaster data and post-disaster

image [3,32,53,54]. However, some errors still exist and may be attributed to two reasons. One is the influence of mixed pixels. Mixed pixels blur the road boundary which further affects the accuracy of damage detection. The other is the influence of trees, vehicles and other landmarks which present different spectra as road and may falsely be classified as the damaged region (Figure 11).

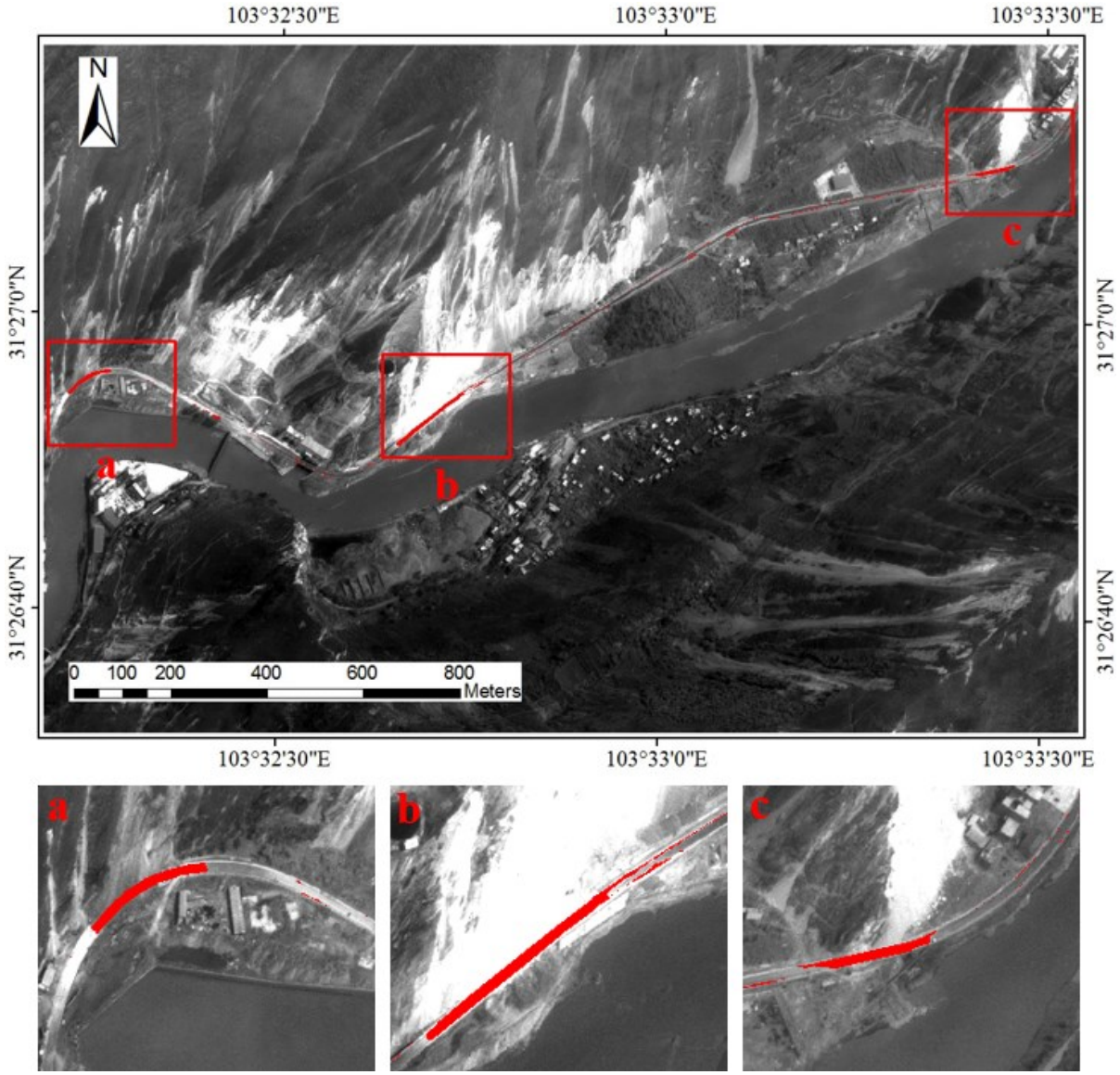

Figure 10. Results of damage detection. Red regions are the damaged road segments.

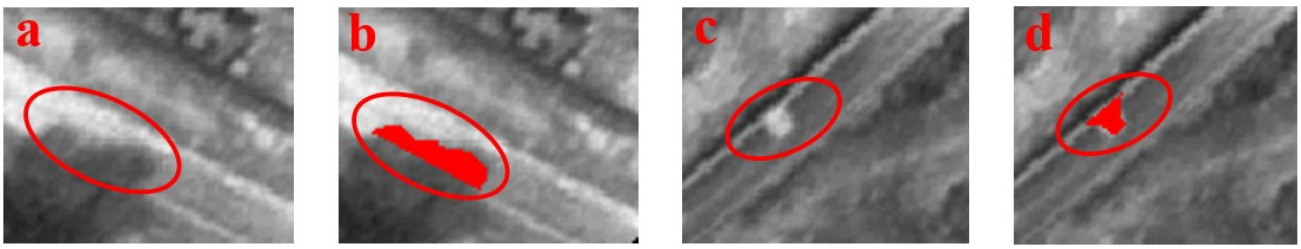

Figure 11. Tree and vehicle that are mistaken as damaged roads. (**a**) Tree shadow; (**b**) Tree shadow is mistaken as damaged road; (**c**) Vehicle; (**d**) Vehicle is mistaken as damaged road.

4.3. Parameter Selection and Sensitivity Analysis

In the proposed road damage detection method, most parameters are estimated automatically, and a few parameters such as image resolution, segmentation scale are set according to the characteristics of the input image. However, there are some manually adjusted parameters in the newly proposed method. To select these parameters, the sensitivity analysis of the newly proposed method is conducted according to the variations of each parameter within reasonable range while other parameters are fixed at the mean value of their ranges [55]. In order to evaluate the free parameter, the following widely accepted evaluation measure [39] is used.

$$\text{Quality (Q)} = \frac{TP}{TP + FN + FP} \tag{11}$$

where *TP* is the damaged road pixels extracted by the proposed method which are consistent with the reference data, *FN* is the damaged road pixels which are in the reference data but not in the extracted result, and *FP* is the extracted damaged road pixels which are not in the reference data. The quantitative results for the free parameters are shown in Figure 12, which compares several reasonable values of b_1, b_2, s_1, s_2, r_1 and w_1 (Section 2.2).

According to the experiments, the values of b_1, b_2, s_1, s_2, r_1 and w_1 are set as 90, 155, 6, 10, 0.5 and 2, respectively. Then, the number (n) of closing operation is to be determined. The principle is the same as that of the aforementioned six parameters selection, but at this time it is automatically selected. As the number (n) increases, the Quality (Q) increases at first, and then decreases. The n is automatically assigned starting from 1 with the step-length of 1. When the Q reaches the local maximum, the corresponding n is selected as the threshold value. In this way, 3 is selected as the threshold value in this paper.

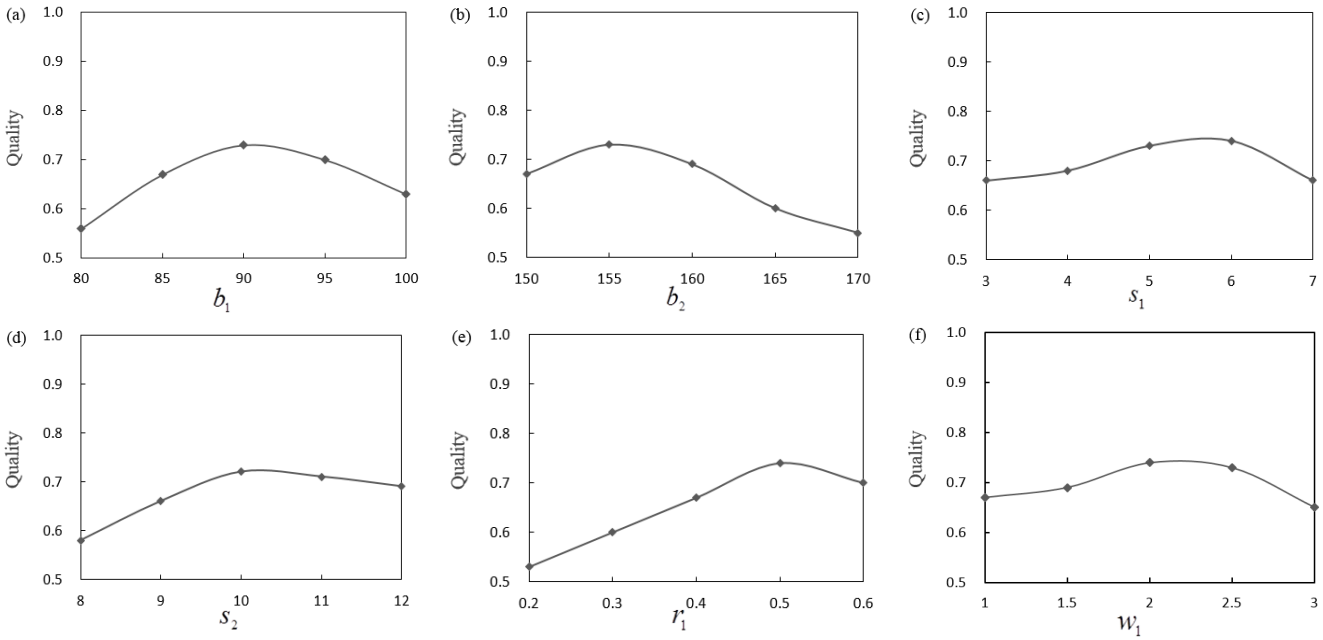

Figure 12. Sensitivity test of free parameters. (**a**) the brightness threshold b_1; (**b**) the brightness threshold b_2; (**c**) the standard deviation threshold s_1; (**d**) the standard deviation threshold s_2; (**e**) the rectangularity threshold r_1; (**f**) the length-to-width ratio threshold w_1.

4.4. Road Damage Assessment

In order to assess the road damage degree, we calculate the indicators of road damage assessment based on the results of road damage detection. Then, the standard of road damage grade specified in Section 2.5 is applied for damage assessment. The result is shown in Figure 13.

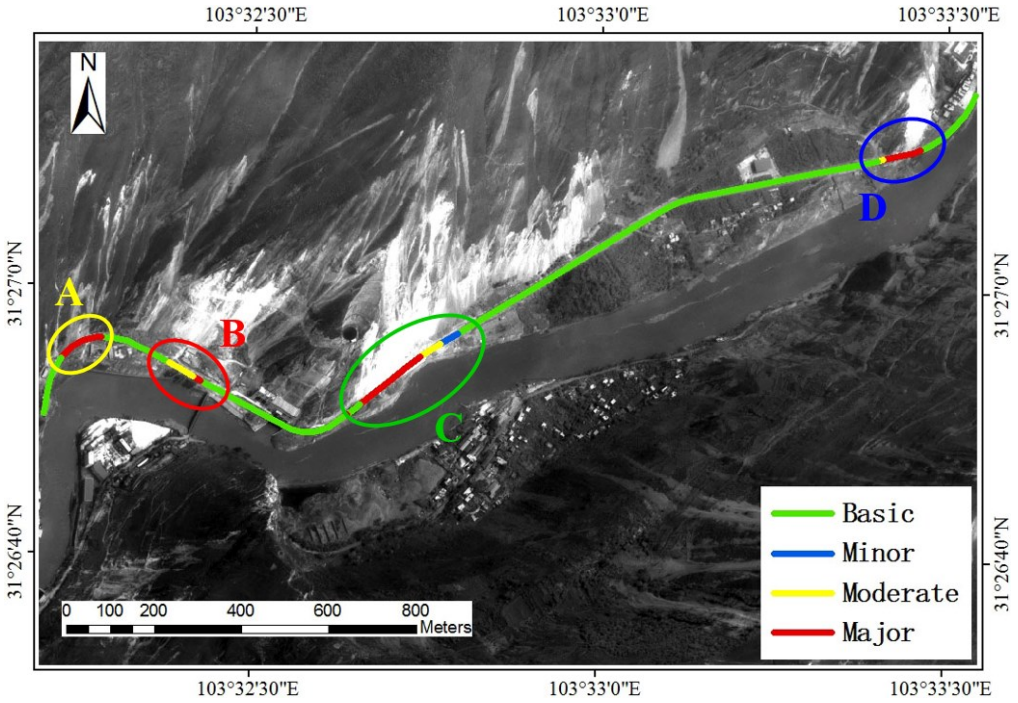

Figure 13. Result of damage grade identification. The damage grades of the green, blue, yellow and red road segments are basic, minor, moderate and major, respectively.

It can be seen from Figure 13 that the damaged road segments are located in four regions. Influenced by the trees and sediments, the damage detected in region B includes some errors. The blue, yellow and red road segments in region A, C and D are correctly detected and actually damaged. The blue road segments are partially buried by landslides or mudslides and they need to be cleaned up. There are some localized cracks in the yellow road segments which require repair. The red road segments have lost the pavement structure, and the traffic capacity of this section has been damaged severely. The repair cost of red road segments is large and rebuilt is required after clean up.

5. Conclusions

In this paper, we focus on road damage detection and assessment without the pre-disaster data, and propose a knowledge-based method using high-resolution optical remote sensing images for a practical application.

One significant novelty of this approach is using the extracted road centerline to substitute the pre-disaster data. For the condition where only the post-disaster image is available, the road centerline is extracted based on the road seed points prescribed by users, which avoids the influence of the absence of pre-disaster data.

Another novelty of this approach is the hypothesis and verification model built based on the road knowledge for post-disaster road extraction. In order to assess the damaged roads, the indicators of damage assessment are built according to the actual road capacity. The standard of road damage grade (basic, minor, moderate and major) is set using the indicators.

Experiments show good results in the evaluation of WorldView-1 image used in Wenchuan Earthquake road damage detection. The producer's accuracy and user's accuracy reach about 90% and 85%, respectively. It is of great value for damaged road detection and assessment in disaster areas especially where pre-disaster data are hard to obtain. Considering the influence of mixed pixels, research on target enhancing algorithms to increase the contrast between the road and other land markers is worth further exploration.

Acknowledgments

This study was funded by the National High Technology Research and Development Program ("863"Program) of China (Grant Number 2012AA121305). We would like to thank anonymous reviewers for their constructive comments, which greatly improved the quality of our manuscript.

Author Contributions

The concept of this study was conceived by Jianhua Wang and Qiming Qin. The experiments were carried out by Jianhua Wang, who also prepared the figures. This manuscript was written by Jianhua Wang, Jianghua Zhao and Xin Ye. The manuscript was revised by Jianhua Wang, Xiao Feng, Xuebin Qin and Xiucheng Yang.

Conflicts of Interest

The authors declare no conflict of interest.

References

1. Plank, S. Rapid damage assessment by means of multi-temporal SAR—A comprehensive review and outlook to sentinel-1. *Remote Sens*. **2014**, *6*, 4870–4906.
2. Lan, R.; Feng, B.; Wang. Z. Study on the fast assessment of traffic capacity of highway bridges after strong earthquakes. *World Earthq. Eng.* **2009**, *25*, 81–87.
3. Li, P.; Xu, H.; Song B. a novel method for urban road damage detection using very high resolution satellite imagery and road map. *Photogramm. Eng. Remote Sens.* **2011**, *77*, 1057–1066.
4. Pitilakis, K.; Alexoudi, M.; Argyroudis, S.; Monge, O.; Martin, C. Earthquake risk assessment of lifelines. *Bull. Earthq. Eng.* **2006**, *4*, 365–390.
5. Li, B. Discussion of the content and assessment criteria of post-disaster bridge in Wenchuan Earthquake. *Southwest Highway* **2008**, *4*, 50–56.
6. Saito, K.; Spence, R.; Going, C.; Markus, M. Using high-resolution satellite images for post-earthquake building damage assessment: A study following the 26 January 2001 Gujarat Earthquake. *Earthq. Spectra* **2004**, *20*, 145–169.

7. Shinozuka, M.; Feng, Q.; Kim, H.; Ueda, T. *Statistical Analysis of Fragility Curves*; Multidisciplinary Center for Earthquake Engineering Research, University of New York: New York, NY, USA, 2001.
8. Chesnel, A.L.; Binet, R.; Wald, L. Object oriented assessment of damage due to natural disaster using very high resolution images. In Proceedings of the IEEE International Conference on Geoscience and Remote Sensing Symposium, Barcelona, Spain, 23–28 July 2007; pp. 3736–3739.
9. Qu, G.; Gao, Q.; Yang, H. Some urgent problems in natural disaster evaluation in China. *Earth Sci. Front.* **1996**, *2*, 212–218.
10. Fan, Y.; Yang, S.; Wang, L. Study on urgent monitoring and assessment in Wenchuan Earthquake. *J. Remote Sens.* **2008**, *12*, 858–864.
11. Zhou, G.; Lu, Y.; Fei, M.; Hu, K.; Qian, J. Research on primary evaluation of earthquake Disaster loss. *J. Seismol. Res.* **2010**, *25*, 208–215.
12. Zhang, J.; Li, J.; Pan, B. Rapid assessment techniques for post-earthquake bridges in China. *J. Highway Transp. Res. Dev.* **2012**, *29*, 51–58.
13. Department of Homeland Security Federal Emergency Management Agency. *Hazus-MH Earthquake Model User Manual*; Federal Emergency Management Agency: Washington, DC, USA, 2012.
14. University of Kentucky. *Post-earthquake Investigation Field Manual for the State of Kentucky*; Kentucky Transportation Center: Lexington, KY, USA, 2006.
15. University of Washington. *Proposed Post-earthquake Bridge Inspection Procedures for New York State*; New York State Department of Transportation: Washington, DC, USA, 2010.
16. Purdue University. *Field Guide for the Post-earthquake Safety Evaluation of Bridges and Roads*; Indiana Department of Transportation: West Lafayette, IN, USA, 2000.
17. Gao, H. Japan's disaster early warning and assessment system. *J. Chin. Acad. Soc.* **2008**, *3*, 1–2.
18. Highway Association of Japan. *Brief Guide of Highway Earthquake Countermeasures* (*Post-Earthquake Emergency Treatment*); Maruzen Co., Ltd.: Tokyo, Japan, 2006.
19. Zhao, Y.; Wang, Y.; Liu, W.; Niu, Y.; Huang, M.; Zhao, Y. The earthquake disaster prediction and evaluation method of the highway system based on fuzzy comprehensive evaluation. *World Earthq. Eng.* **2010**, *26*, 139–144.
20. Amelia, M.; Hannah, E.; Jody, M.; Ana, V. Evolution of coral rubble deposits on a reef platform as detected by remote sensing. *Remote Sens.* **2013**, *5*, 1–18.
21. Wang, J.; Qin, Q.; Yang, X.; Wang, J.; Ye, X.; Qin, X. Automated road extraction from multi-resolution images spectral information and texture. In Proceedings of the IEEE International Conference on Geoscience and Remote Sensing Symposium, Québec, Canada, 13–18 July 2014; pp. 533–536.
22. Kaur, A.; Singh, R. Various methods of road extraction from satellite images: A review. *Int. J. Res.* **2015**, *2*, 1025–1032.
23. Li, Y.; Xu, L.; Piao, H. Semi-automatic road extraction from high-resolution remote sensing image: Review and prospects. In Proceedings of the 2009 IEEE Ninth International Conference on Hybrid Intelligent Systems, Shenyang, China, 12–14 August 2009, volume 1, pp. 204–209.
24. Callier, S.; Saito, H. Automatic road area extraction from printed maps based on linear feature detection. *IEICE Trans. Inf. Syst.* **2012**, *95*, 1758–1765.

25. Anil, P.; Natarajan, S. Automatic road extraction from high resolution imagery based on statistical region merging and skeletonization. *Int. J. Eng. Sci. Technol.* **2010**, *2*, 165–171.
26. Mokhtarzade, M.; Zoej, M. Road detection from high-resolution satellite images using artificial neural networks. *Int. J. Appl. Earth Obs. Geoinf.* **2007**, *9*, 32–40.
27. Trinder, J.; Wang Y. Knowledge-based road interpretation in aerial images. *Int. Arch. Photogramm. Remote Sens.* **1998**, *32*, 635–640.
28. Senthilnath, J.; Rajeshwari, M.; Omkar, S. Automatic road extraction using high resolution satellite image based on texture progressive analysis and normalized cut method. *J. Indian Soc. Remote Sens.* **2009**, *37*, 351–361.
29. Singh, P; Garg, R. Automatic road extraction from high resolution satellite image using adaptive global thresholding and morphological operations. *Indian Soc. Remote Sens.* **2013**, *3*, 631–640.
30. Teng, X.; Song, S.; Zhan, Y. A novel road extraction algorithm for high resolution remote sensing images. *Appl. Math. Inf. Sci.* **2014**, *8*, 1435–1443.
31. Gong, L.; An, L.; Liu, M.; Zhang, J. Road damage detection from high-resolution RS image. In Proceedings of the IEEE International Conference on Geoscience and Remote Sensing Symposium, Munich, Germany, 22–27 July 2012, pp. 990–993.
32. Ma, H. Research on Road Damage Detection from High Resolution Remotely Sensed Images for Disaster Evaluation. Ph.D. Theses, Peking University, Beijing, China, 13 June 2009.
33. Qin, Q.; Ma, H.; Li, J. Damage detection and assessment system of roads for decision support for disaster. *Key Eng. Mater.* **2011**, *467–469*, 1144–1149.
34. Earthquake Destruction Assessment of Urban Roads Network Using Satellite Imagery and Fuzzy Inference Systems. Available online: http://www.isprs.org/proceedings/XXXVII/congress/8_pdf/2_WG-VIII-2/47.pdf (accessed on 22 April 2015).
35. Wang, Y.; Wang, Y.; da, Y.; Liu, X.; Li, J.; Huang, J. An object-oriented method for road damage detection from high resolution remote sensing images. In proceedings of the 19th International Conference on GeoInformatics, Shanghai, China, 24–26 June 2011, pp. 1–5.
36. Haghighattalab, A.; Mohammadzadeh, A.; Valadan Zoej, M.; Taleai, M. Post-earthquake road damage assessment using region-based algorithms from high-resolution satellite images. *Proc. SPIE* **2010**, *7830*, doi:10.1117/12.864538.
37. Shi, W.; Miao, Z.; Debayle, J. An integrated method for urban main road centerline extraction from optical remotely sensed imagery. *IEEE Trans. Geosci. Remote Sens.* **2014**, *52*, 3359–3372.
38. Miao, Z.; Shi, W.; Zhang, H. Road centerline extraction from high-resolution imagery based on shape features and multivariate adaptive regression splines. *IEEE Geosci. Remote Sens. Lett.* **2013**, *10*, 583–587.
39. Miao, Z.; Wang, B.; Shi, W. A semi-automatic method for road centerline extraction from VHR images. *IEEE Geosci. Remote Sens. Lett.* **2014**, *11*, 1856–1860.
40. Peyré, G.; Péchaud, M.; Keriven, R.; Cohen, L. Geodesic methods in computer vision and graphics. *Trends Comput. Graphics Vis.* **2010**, *5*, 197–397.
41. Hastie, T.; Tibshirani, R.; Friedman, J. *The Elements of Statistical Learning: Data Mining, Inference, and Prediction*, 2nd Ed.; Springer-Verlag: Berlin, Germany, 2008.
42. Ahamada, I.; Flachaire, E. *Non-Parametric Econometrics*; Oxford Univ. Press: Oxford, UK, 2010.

43. Cheng, Y. Mean shift, mode seeking, and clustering. *IEEE Trans. Pattern Anal. Mach. Intell.* **1995**, *17*, 790–799.
44. Paris, S.; Kornprobst, P.; Tumblin, J.; Durand, F. Bilateral filtering: Theory and applications. *Found. Trends Comput. Graph. Vis.* **2008**, *4*, 1–73.
45. Canny, J. A Computational approach to edge detection. *IEEE Trans. Pattern Anal. Mach. Intell.* **1986**, *PAMI-8*, 679–698.
46. Li, J.; Qin, Q.; Ma, H.; Yuan, W. Study on road damage assessment based on RS and GIS. In Proceedings of 2010 IEEE International Geoscience and Remote Sensing Symposium (IGARSS), Honolulu, HI, USA, 25–30 July 2010, doi:10.1109/IGARSS.2010.5651949.
47. Liu, W.; Hu, H.; Cheng, C.; Li, Q. Application of grey correlation degree to disaster loss evaluation of strong wind and heavy rainfall. *Meteorol. Sci. Technol.* **2007**, *4*, 563–566.
48. Dilley, M.; Chen, R.S.; Deichmann, U.; Lerner-Lam, A.L.; Arnold, M. *Natural Disaster Hotspots: A Global Risk Analysis*; International Bank for Reconstruction and Development; The World Bank and Columbia University: Washington, DC, USA, 2005.
49. Rivas, V.; Rix, K.; Frances, E. Cendrero, A.; Brunsden, D. Geomorphological indicators for environmental impact assessment: Consumable and non-consumable geomorphological resources. *Geomorphology* **1997**, *18*, 169–182.
50. Stuart, D.; Sungbin, C.; Ronald, T. *The Shakeout Scenario Supplemental Study: Analysis of Risks to Southern California Highway System*; SPA Risk LLC: Oakland, CA, USA, 2008.
51. GB/T 18208.4–2011. *Post-earthquake Field Works—Part 4: Assessment of Direct Loss*; China Earthquake Administration: Beijing, China, 2011.
52. Chen, C. Recognition and Damage Assessment for Bridge over Water from High-resolution Optical Remote Sensing Images. Ph.D. Theses, Peking University, Beijing, China, 9 June 2013.
53. Ma, H.; Lu, N.; Ge, L.; Li, Q.; You, Z.; Li, X. Automatic road damage detection using high-resolution satellite images and road maps. In Proceedings of the 2013 IEEE International conference on Geoscience and Remote Sensing Symposium, Melbourne, Australia, 21–26 July 2013; pp. 3718–3721.
54. Kawamura, M.; Tsujino, K.; Shimada, T.; Tsujiko, Y. Disaster damage detection and its recovery support system of road and railroad using satellite images. *Int. Arch. Photogramm. Remote Sens. Spat. Inf. Sci.* **2010**, *8*, 314–319.
55. Gao, C.; Sun, Y. Automatic road centerline extraction from imagery using road GPS data. *Remote Sens.* **2014**, *6*, 9014–9033.